Applied Magnetic Resonance (2020) 51:939–949
https://doi.org/10.1007/s00723-020-01254-6

Applied
Magnetic Resonance

ORIGINAL PAPER

Radical Activity of Binary Melamine-Based Hydrogen-Bonded Self-Assemblies

Vladimir V. Shilovskikh[1] · Alexandra A. Timralieva[1] · Elena V. Belogub[2] · Elizaveta A. Konstantinova[3] · Alexander I. Kokorin[4,5] · Ekaterina V. Skorb[1]

Received: 12 July 2020 / Revised: 5 August 2020 / Published online: 3 September 2020

Abstract

Melamine cyanurate and melamine barbiturate self-assembled materials were prepared and studied by the electron paramagnetic resonance (EPR) spectroscopy, optical and scanning electron microscopy, X-ray powder diffraction (XRD). Both optical and electron microscopy show the formation of microscale crystalline particles possessing complex layered structures with a highly stable appearance. Both assemblies tend to form twinned crystals, which in the barbiturate case leads to multiple twinning in every particle. Optical microscopy shows high anisotropy and birefringence of both materials. XRD data represent a high crystallinity of melamine barbiturate and much lower for melamine cyanurate. Studied materials reveal the ability to incorporate radicals that correlate with their crystal structure quality. It is attributed to the structure-dependent stabilization of active radical superoxide species in structure voids or defects. In the example of melamine barbiturate, it is shown that the number of active paramagnetic centers increases at *ca*. 22% when a substance is irradiated with UV + Vis light. It reaches saturation in approximately 20 min, whereas only *ca*. 14% decrease was observed in a week.

✉ Vladimir V. Shilovskikh
vvshlvskh@gmail.com

[1] Infochemistry Scientific Center, ITMO University, Lomonosova str. 9, Saint Petersburg 191002, Russia

[2] South Urals Federal Research Center of Mineralogy and Geoecology, Urals Branch of Russian Academy of Science, Miass 456317, Russia

[3] Department of Physics, M. V. Lomonosov Moscow State University, Moscow, Russia

[4] N.N. Semenov Federal Research Center for Chemical Physics, Russian Academy of Sciences, Moscow, Russia

[5] Plekhanov Russian University of Economics, Moscow, Russia

1 Introduction

The pronounced radical activity of substances that do not exhibit homolytic bond break at mild stress and do not produce radicals themselves is an intriguing question. Such behavior may result from several causes, such as intensive irradiation of biological samples [1], or paramagnetic probe injection [2]. Such injection of a sensitive probe into a structure is a powerful method of the local structure investigation. For example, semiconductor silicon surface bombardment with protons [3] reveals not only a number, but also a local surrounding of defects and their type. Not only that, crystals are known to stabilize radical states and significantly change their properties [4]. Electron paramagnetic resonance (EPR) studies of glasses treated with ion irradiation make it possible to identify ion surroundings and, therefore, to describe prevailing local glass microstructures [5]. EPR signal of a stable crystalline structure doped with EPR-active ions is sensitive to the geometry of incorporated admixture and gives an insight into forces, stabilizing their structures [6]. Spin labels can even be used to solve microstructural problems for such dynamic structures as ionic liquids [7]. Thus, magnetic spectroscopy methods could provide substantial information for investigation of structural and dynamic peculiarities of a wide array of complex systems. We propose two host–guest systems able to encapsulate active oxygen species and accordingly active in EPR.

Melamine cyanurate (M-CA) is one of the most stable organic self-assemblies. Its structure consists of infinite hexagonally packed layers (Fig. 1a) composed of altering melamine (Fig. 1c) and cyanuric acid (Fig. 1d) molecules. Each molecule is connected with three neighbors with rigid triple hydrogen bonds [8]. Layers are

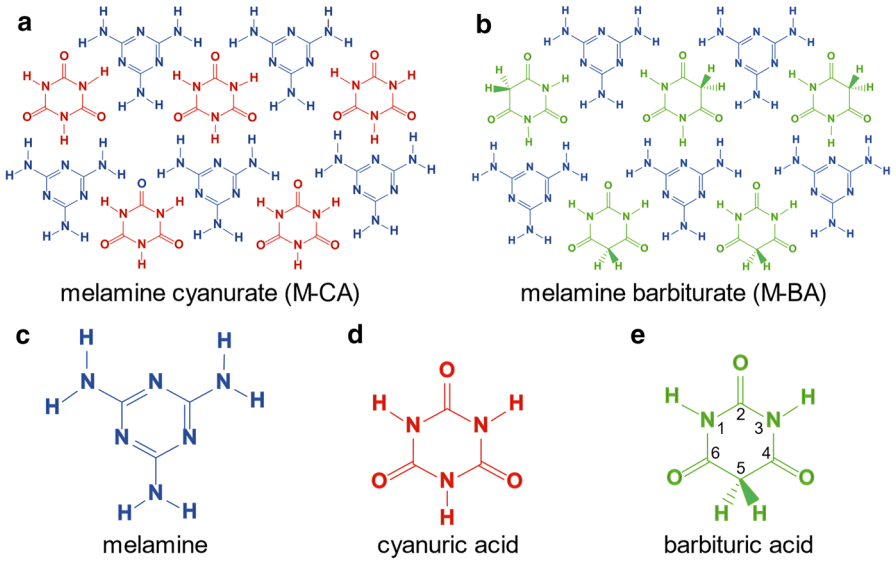

Fig. 1 Schematic structure of M-CA sheets (**a**), M-BA sheets (**b**), structural formulas of melamine (**c**), cyanuric (**d**), and barbituric acid (**e**). The order of numbering of atoms in the ring is indicated for the latter case

stacked one over another and held together mostly by hydrophobic interactions and π-stacking [9]. The extra stability of M-CA symmetric structure leads both to the extremely low solubility of a compound in water or unipolar solvents and to an instant formation of a fine powdery suspension of stoichiometric M-CA at concentrations less than 10^{-4} M. This ability is used as an analytical reaction for both qualitative and quantitative determination for both reagents [10].

Melamine barbiturate (M-BA) (Fig. 1b) is a close analog of M-CA in the nature of formation. However, it possesses some significant distinctions. The most crucial is the asymmetry of the barbituric acid molecule (Fig. 1e) which leads to lowering the symmetry of 2D sheets composing M-BA crystals [11]. Another significant difference is the acidity of C5 carbon of barbituric acid and accordingly much higher pK_a compared to cyanuric acid [12]. The higher acidity in turn leads to better solvation of an individual molecule. The asymmetry of barbituric acid molecule suggests two unequal directions where a bond between carbon-based hydrogen of barbituric acid with melamine is much weaker than that of nitrogen-based hydrogen. The inequality of the attachment modes of a new molecule to the crystal's surface may lead to the emergence of unoccupied sites in the structure and generation of active centers capable of specific adsorption, such as cationic or radical incorporation, into the structure. The third significant distinction is a high (up to 10^{-3} mol/l) solubility which allows recrystallization processes and defects healing during crystal growth.

Neither cyanuric nor barbituric acid, or melamine is reported to reveal any significant radical activity in a free state and, thus, an EPR activity of their structure is attributed to structural effects of their binary self-assemblies. Therefore, the EPR investigation of these systems was the main aim of this work.

2 Experimental

Barbituric acid (C4H4N2O3, 99.0%, Sigma Aldrich), cyanuric acid (C3H3N3O3, 99.0%, Sigma Aldrich), and melamine (C3H6N6, 99.0%, Sigma Aldrich) were purchased and used without further purification. Deionized water was used as a solvent. 20 mM solutions of melamine, cyanuric, and barbituric acids in water were prepared in advance. Powders were precipitated from solutions in 1:1 volumetric ratios. When solutions were mixed, an opaque insoluble precipitate is formed. All the samples were centrifuged, the supernatant was drained and the resulting powders washed with deionized water three times, then dried on air. Three sets of experiments were performed to confirm the reproducibility of the results.

X-ray powder diffraction (XRD) data of melamine barbiturate and melamine cyanurate were collected by Shimadzu XRF 600 with Cu Kα radiation from diffraction-less silicon as a substrate with a speed of 1 degree per min. All calculations were made using regular Shimazu software.

Scanning electron microscopy (SEM) studies were performed with a Tescan Vega scanning electron microscope. Optical photos were acquired at Leica 4500P and Zeiss Axioscope A1 equipped with UV source.

The EPR spectra were recorded at room temperature with a Bruker spectrometer ELEXSYS-E500 (*X*-band, the sensitivity up to 1011 spin/G). Parameters of the

spectrometer were set as follows: modulation frequency, MF = 9.662 GHz, modulation power, MP = 0.2 mW, modulation amplitude, MA = 2.00 G, due to the line width of each single line was ca. 7.0 G.

For investigating the photoactivity and behavior of paramagnetic centers (PCs), the samples were illuminated directly in the cavity of the spectrometer with the use of 50 W high-pressure mercury lamp. The concentration of PCs was evaluated using $CuCl_2 \times 2H_2O$ monocrystal with a known number of spins as the standard. From the EPR spectra, *g*-factor values and line widths ΔH of the observed PCs were determined using a computer program package developed and kindly provided by Prof. A. Kh. Vorob'ev (Chemistry Department, M. Lomonosov Moscow State University) [13].

3 Results and Discussion

Two sets of powders were prepared in aqueous solutions and dried. All the samples were studied using optical and electron microscopy. Both methods show significant distinctions in particle appearances. M-CA forms spindle-like elongated particles 0.2–0.5 μm in width and up to 20 μm in length. Twinning is detected for a small fraction of crystals (Fig. 2a), slight cleavage is observed at high magnification (Fig. 2c). M-BA forms highly twinned star-shaped polycrystalline aggregates with smooth edges with a size of 20–100 μm and no expressed cleavage (Fig. 2b, d).

The particles possess similar shapes which indicates the existence of a single structural type and, accordingly, the formation in a single ratio of components. To determine this ratio, we used the acid–base properties of M ($pK_a = 5.0$) [12], CA ($pK_{a1} = 6.88$) [14] and BA ($pK_{a1} = 4.01$) [15]. Any reaction between them will expend components and, accordingly, affect the pH of the medium. Titrating one component with another, titration jumps should be observed when the content of the components is equal to the ratio necessary for the formation of the compound. Such titrations show the existence of a single inflection point on the curves starting both from melamine or acid solution. All inflection points correspond to 1:1 ratios (Fig. 3). The case of barbituric acid has peculiar points in the first moments of titration, associated with a delay in the formation of particles. This may be due to the existence of a kinetically inhibited nucleation stage [16].

Imaging in a polarized light shows lingering crystalline orientation within a single grain, distinct anisotropy, and high birefringence. Color zonation of particles in polarized light for M-CA is caused by light interference in thin films (Fig. 4a). Polarized light also shows anisotropy and a high birefringence (Fig. 4c).

Luminescent microscopy shows weak luminescence in a blue region. The intensity distribution is uniform in M-CA particles (Fig. 4c), whereas M-BA particles demonstrate an increase in luminescence towards the ends of the crystals (Fig. 4d). Diffusion-driven model of the particle growth suggests a gradual decrease in growth speed [17] up to a point where the growth rate is equal to a dissolution rate. Local depletion of the feeding solution in the dissolved substance in turn leads to a free Gibbs energy of the process decrease following Van't Hoff isotherm equation. This phenomenon can also be accompanied by

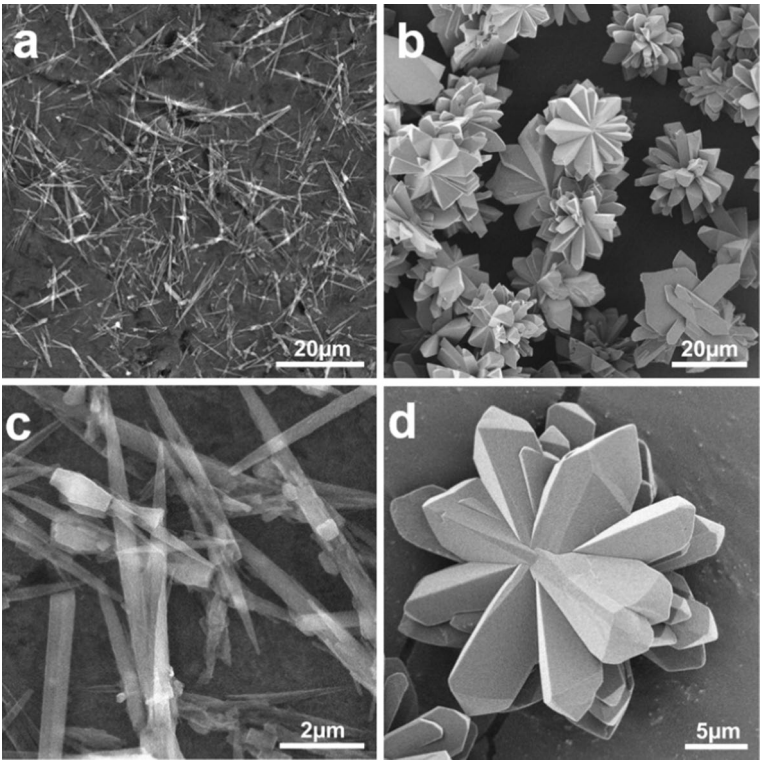

Fig. 2 SEM images: **a**, **c** M-CA crystals; **b**, **d** M-BA crystals

a higher-impurity incorporation rate. It can be described by the relative slowdown of the main reaction of a particle's growth while competing impurity capture reaction rate remains the same. In a certain range of reaction conditions, the impurity capture process may take on an oscillatory appearance [18].

The spatial non-uniformity of luminescence within one M-BA particle may indicate two different scenarios. Either this ability is greatly influenced by external environmental factors or even it is not an integral characteristic of the material at all but is caused by some external factor. It has been suggested that, during growth, a particle can trap and accommodate impurities from the solution.

EPR spectra were recorded for the samples. In both cases, a signal is detected (Fig. 5). Positions of the signals are found at $g \approx 2.003 \pm 0.002$ and their shape is characteristic of organic radicals similar to those observed in [19]. Similar radicals were attributed as products of the homolytic braking of C–H or C–C bonds in organic compounds in [20, 21]. A signal of the empty resonator denoted with a star in Fig. 5 can be used as a reference with $g_0 = 2.000$. The spectrum of M-BA is shown for the comparison (Fig. 5c). One can see that the number of spins (PCs) noticeably depends on the sample. The spectrum of M-BA in Fig. 5 has been recorded with one scan, while for both M-CA spectra, a six-scan accumulation was used, and also the

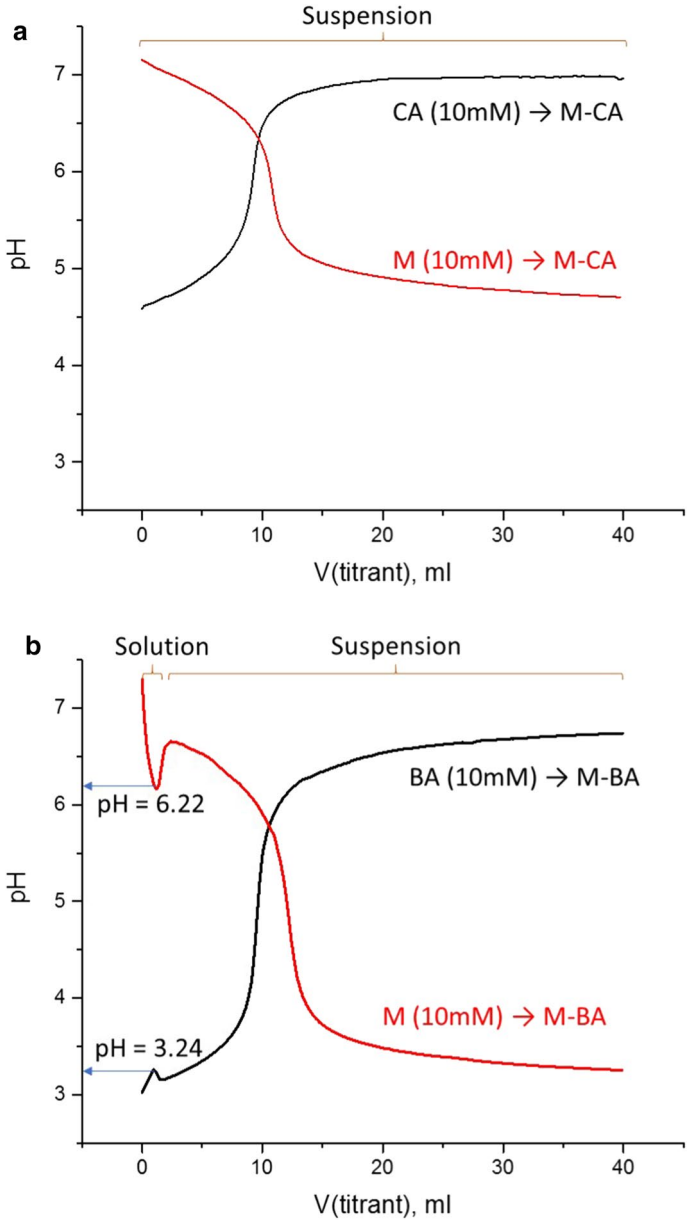

Fig. 3 **a** Potentiometric curve of titration of melamine by cyanuric acid (red line) and vice versa (black line); **b** Potentiometric curve of titration of melamine by barbituric acid (red line) and vice versa (black line) (colour figure online)

receiver gain coefficient was increased threefold. Considering this, the content of radicals in M-BA determined as 5×10^{16} spin/g, we can estimate such value of PCs in M-CA, $[R]_0$, as *ca*. 6×10^{14} spin/g, i.e., rather negligible compared to M-BA.

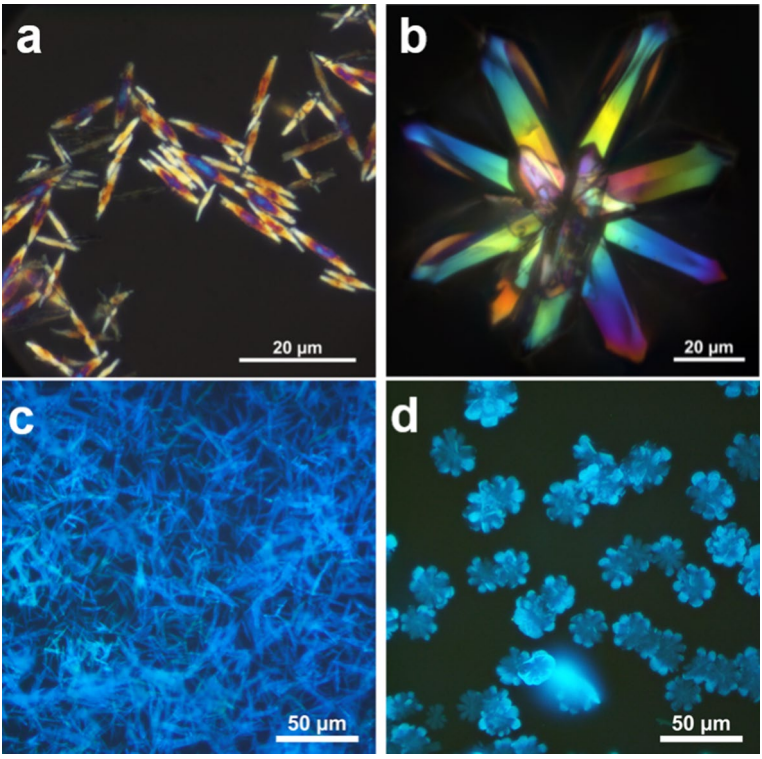

Fig. 4 **a**, **b** M-CA and M-BA crystals, respectively, in polarized light; **c**, **d** M-CA and M-BA crystals luminescence

Comparing EPR spectra of the M-CA to M-BA, we observed g-factor coincidence within the margin of error; however, M-BA demonstrated two orders of magnitude higher signal intensity. Due to low intensity and small signal-to-noise ratio, we did not detect the influence of UV–Vis light irradiation on the radical concentration after 16 min of illumination (see Fig. 5b) in contrast to M-BA. M-BA EPR spectrum intensity is significantly increased under UV–Vis irradiation with rather small changes of the spectrum shape seeing in Fig. 5. Signal intensity increases by *ca*. $14 \pm 2\%$ and reaches saturation after approximately 20 min of illumination (Fig. 6, inset). We suppose further intensity increase is offset by radical recombination processes, i.e., by achieving the generation-recombination equilibrium.

Irradiated samples being held in dark conditions just after stopping light exposure show a very slow decrease of the EPR signal intensity; after 7 days, it did not achieve the initial level. This dramatic difference in speed means that M-BA accommodates and stabilizes radical species. However, such accommodation does not include significant electronic interactions with M-BA, especially with nitrogen atoms, since no signs of the signal splitting caused by hyperfine interaction with ^{14}N nuclei (the nonzero spin $I^{N} = 1$) are detected. As well as in case of M-BA for M-CA, no hyperfine interaction is observed.

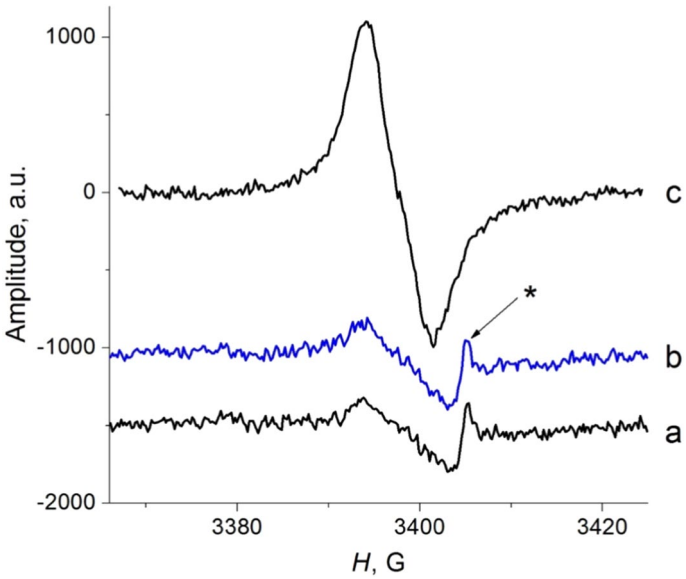

Fig. 5 EPR spectra at 298 K of M-CA initial (a), after 20 min of UV + Vis light irradiation (b), and M-BA in dark (c). A star depicts a line of the EPR cavity signal

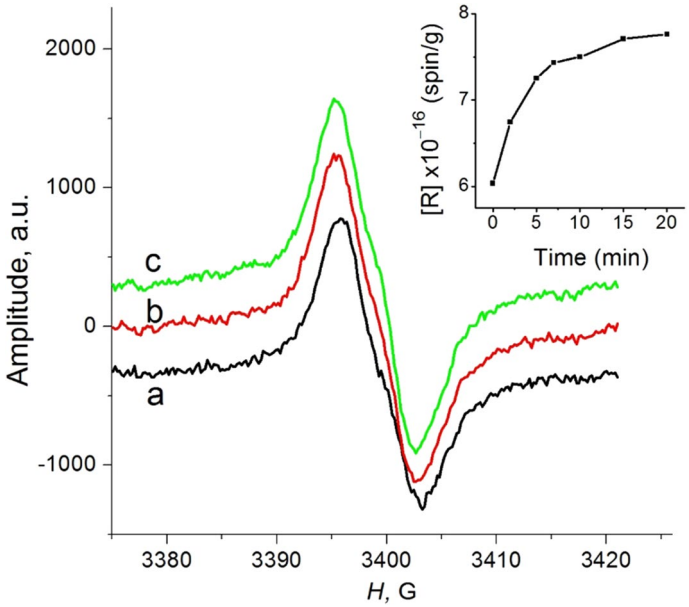

Fig. 6 EPR spectra of M-BA initial (a) and being irradiated with UV + Vis light after 7 (b) and 20 min (c) of exposures. Inset shows the radical accumulation kinetics under light exposure

Neither M-CA nor M-BA contains a part remote from ^{1}H or ^{14}N that they can host the radical generating singlet signal. This is a clear evidence of external source of radical species. Since no other reagent except melamine, cyanuric acid, barbituric acid, water and dissolved oxygen are present in reaction media, we believe that superoxide radical or related oxygen-centered species stabilized in self-assembly structure is responsible for the EPR signal.

Differences in signal strength of M-BA and M-CA are in good accordance with mean particle's size and are opposite to specific surface area value of substances which may be considered as evidence that the EPR signal is generated by a specie that is located in the bulk matrix, and not on the surface of the particle.

To estimate the structural effect, XRD patterns of both M-CA and M-BA were studied (Fig. 7). An assumption was made that the XRD data are not affected by particle sizes because significant peak broadening is observed for crystallites less than 0.2 μm in diameter. M-CA diffraction pattern contains a set of broad peaks. The most intensive corresponds to $d = 8.24$ Å, which is a doubled value of reported interlayer distance for M-CA [9]. There are three repetitions of the peak at doubled and tripled angles which indicate dense layers as a main motif of the structures, whereas other peaks are much less pronounced. The crystallinity parameter calculated based on diffraction peaks shapes for M-CA powder is only 52.6%. The M-BA structure generates a significantly richer XRD pattern, which probably indicates a decrease in the symmetry of the structure, with sharp diffraction peaks. The main peak is close to that one of M-CA and corresponds to $d = 7.93$ Å. Five repetitions are detected at higher angles. The calculated crystallinity parameter is 89.2% and it lays in the range, typical for highly crystalline materials.

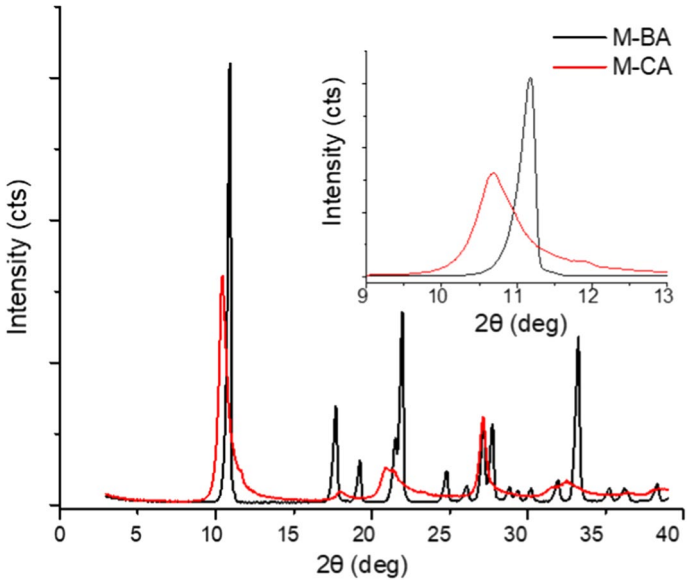

Fig. 7 M-CA (red line) and M-BA (black line) XRD patterns comparison

4 Conclusion

Two self-assembly materials were studied. They were found to form crystalline precipitates in 1:1 ratios and possess similar optical properties, such as anisotropy and birefringence. In the present work, we report surprising luminescent behavior and singlet EPR signals with $g \approx 2.003 \pm 0.002$. UV–Vis light irradiation is found to enhance radical concentration in M-BA from 6×10^{16} to 7.8×10^{16} spin/g in 20 min of illumination. Relaxation is significantly slower and the intensity does not reach the initial level even after leaving the sample for 7 days in the dark. XRD data analysis shows higher crystallinity of the sample with higher intensity of the EPR signal. We associate this behavior and the appearance of the EPR activity with accommodation of radicals in the layered structure of self-assemblies in interlayer space or structure voids with no direct electron exchange with M-CA or M-BA itself.

Acknowledgements This work is supported by the Ministry of Science and Higher Education of the Russian Federation, goszadanie no. 2019-1075. ITMO Fellowship and Professorship program 08-08 is acknowledged for infrastructural support.

Data Availability All data available from the corresponding author on request.

Compliance with Ethical Standards

Conflict of interest Authors declare no conflicts of interest.

References

1. P. Fattibene, F. Callens, Appl. Radiat. Isotopes **68**, 2033–2116 (2010)
2. C.-T. Yang, A. Hattiholi, S.T. Selvan, S.X. Yan, W.-W. Fang, P. Chandrasekharan, P. Koteswaraiah, C.J. Herold, B. Gulyas, S.E. Aw, T. He, D.C.E. Ng, P. Padmanabhan, Acta Biomater. **110**, 15–36 (2020)
3. Y.V. Gorelkinskii, N.N. Nevinnyi, Phys. B: Condensed Matter **170**, 155–167 (1991)
4. J. Xiong, J. Di, J. Xia, W. Zhu, H. Li, Adv. Funct. Mater. **180**, 2018 (1983)
5. L.D. Bogomolova, V.A. Jachkin, S.A. Prushinsky, S.V. Stefanovsky, Y.G. Teplyakov, F. Caccavale, J. Non-Cryst. Solids **220**, 109–126 (1997)
6. M.A. Borik, R.M. Eremina, E.E. Lomonova, V.A. Myzina, V.V. Osiko, I.I. Fazlizhanov, V.A. Shustov, I.V. Yatsyk, Mod. Electron. Mater. **3**, 95–98 (2017)
7. M.Y. Ivanov, M.V. Fedin, Mendeleev Commun. **28**, 565–573 (2018)
8. G. Whitesides, J. Mathias, C. Seto, Sci. **254**, 1312–1319 (1991)
9. T.J. Prior, J.A. Armstrong, D.M. Benoit, K.L. Marshall, CrystEngComm **15**, 5838 (2013)
10. K. Rovina, S. Siddiquee, J. Food Compos. Anal. **43**, 25–38 (2015)
11. V.V. Shilovskikh, A.A. Timralieva, P.V. Nesterov, A.S. Novikov, P.A. Sitnikov, E.A. Konstantinova, A.I. Kokorin, E.V. Skorb, Chem. Eur. J. **2**, 2 (2020)
12. H.C. Garcia, R. Diniz, M.I. Yoshida, CrystEngComm **11**, 881 (2009)
13. A.Kh. Vorobiev, N.A. Chumakova, *Nitroxides: Theory, Experiment and Applications* (InTech Publ, Rijeka, 2012), pp. 57–112
14. J.B. Weber, Res. Rev. **32**, 93–130 (1970)
15. M.J. O'Neil, J. Am. Chem. Soc. **129**, 2197 (2007)
16. N. Türkel, M.S. Aksoy, ISRN Anal. Chem **2**, 1–5 (2014)
17. J.W.P. Schmelzer (ed.), *Nucleation Theory and Applications* (JINR, Dubna, 2005)

18. K. Sangwa, *Nucleation and Crystal Growth: Metastability of Solutions and Melts* (Wiley, New York, 2018)
19. F. Kalischewski, I. Lubashevsky, A. Heuer, Phys. Rev. E **75**, 2 (2007)
20. C. Zhao, Z. Chen, J. Xu, Q. Liu, H. Xu, H. Tang, G. Li, Y. Jiang, F. Qu, Z. Lin, X. Yang, Appl. Catal. B Environ. **256**, 117867 (2019)
21. E.R. Draper, L.J. Archibald, M.C. Nolan, R. Schweins, M.A. Zwijnenburg, S. Sproules, D.J. Adams, Chem. Eur. J. **24**, 4006–4010 (2018)